Journal of Electroceramics 4:2/3, 369–377, 2000

Pulsed Laser Deposition of $Zr_{1-x}Ce_xO_2$ and $Ce_{1-x}La_xO_{2-x/2}$ for Buffer Layers and Insulating Barrier in Oxide Heterostructures

R. LYONNET,[1] A. KHODAN,[2] A. BARTHÉLÉMY,[1] J.-P. CONTOUR,[1] O. DURAND,[3] J.L. MAURICE,[1] D. MICHEL[4] & J. DE TERESA[1]

[1]*Unité Mixte de Physique C.N.R.S./Thomson-CSF, 91404 Orsay, France*
[2]*Institute of Physical Chemistry, Russian Academy of Sciences, 117915 Moscow, Russia*
[3]*LCR/Thomson-CSF, 91404 Orsay, France*
[4]*C.E.C.M./C.N.R.S., 94407 Vitry sur Seine, France*

Abstract. We have studied the pulsed laser deposition (PLD) of $Zr_{1-x}Ce_xO_2$ and $Ce_{1-x}La_xO_{2-x/2}$ initially to grow buffer layers for perovskite films deposited on Si, $LaAlO_3$, $SrTiO_3$ and MgO and then to produce tunneling barriers for cuprate or manganite heterostructures. On (1 0 0) Si, the deposition of $Zr_{1-x}Ce_xO_2$ ($x = 0.12$) produces a smooth epitaxial layer ($R_{RMS} = 0.25\,nm/1\,\mu m^2$), which allows the further deposition of high quality $YBa_2Cu_3O_7$ ($Tc \geq 88\,K$) and $La_{0.7}Sr_{0.3}MnO_3$ films. On the other hand, the use of $Ce_{1-x}La_xO_{2-x/2}$ ($0 \leq x \leq 0.4$) makes it possible to match the $YBa_2Cu_3O_7$ and $La_{0.7}Sr_{0.3}MnO_3$ layers to various substrates. The buffer layers are epitaxially grown with a 45° rotation of the in-plane axes with respect to those of the substrate, and the smoothness is high ($R_{RMS} = 0.24\,nm/1\,\mu m^2$).

In the case of an ultra-thin barrier ($\cong 2.5\,nm$) of $Ce_{1-x}La_xO_{2-x/2}$ sandwiched in a $La_{0.7}Sr_{0.3}MnO_3$, the out-of-plane mismatch of $\sqrt{2}$ induces distortions at the interface steps, which propagate into the topmost $La_{0.7}Sr_{0.3}MnO_3$ layer. This is in contrast to the case of $SrTiO_3$ barriers where an ideal crystal continuity in the growth direction is observed.

Keywords: high temperature super conductors, magnites, oxide epitaxy, thin films, pulsed laser

Introduction

The epitaxial growth of oxide thin films for the crystal engineering which is needed in some electronic applications of oxide corresponds most of the time to an hetero-epitaxial process in which the substrate and the film generally present different lattice parameters, thermal expansion factor and finally crystal structure [1–3]. An oxide buffer layer may then be necessary in order to minimize the lattice mismatch and/or the thermal expansion coefficient. When the active compound is HTSC cuprate or mixed valence manganese oxide, the main substrates, which are usually used to grow high quality thin films, are: MgO, Al_2O_3 (sapphire), $ZrO_2(Y_2O_3)$, $SrTiO_3$, $LaAlO_3$, $NdGaO_3$, $LaSrGaO_4$. In that case, although the thermal expansion factors are well matched, one can observe a marked mismatch between the lattice parameters, especially for the orthorhombic structure of $YBa_2Cu_3O_7$ [4].

On the other hand, if a silicon substrate is used in order to developp hybrid electronic devices, the thermal expansion factor of the substrate is around 5 times lower than those of the perovskites (Fig. 1). In this case, an yttria-stabilized-zirconia buffer layer, associated sometime with a CeO_2 buffer layer, is usually used in order to compensate for the thermal expansion coefficient and the parameter mismatch [5–8]. However the quality of the substrate/film interface is poor due to the interfacial silicon oxide produced on the surface of the silicon substrate at the first step of the buffer layer growth under oxygen pressure [9]. We report here on the use of a single buffer layer of $Zr_{1-x}Ce_xO_{2-x/2}$ grown from a metallic target under

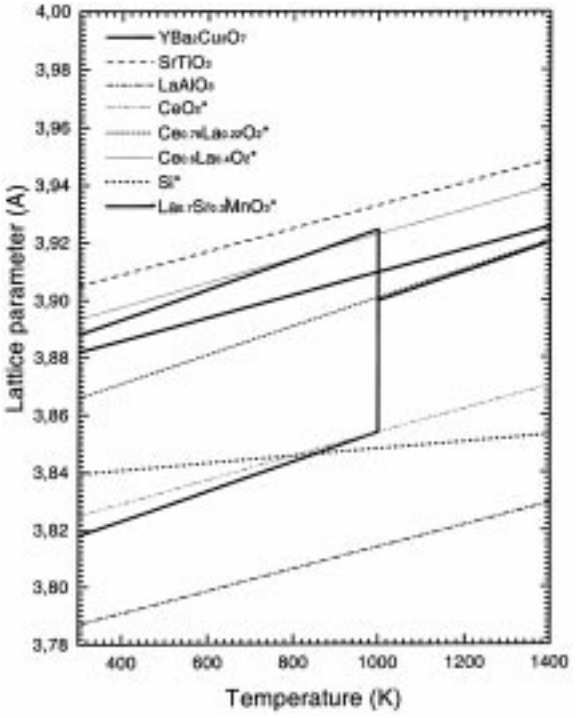

Fig. 1. Lattice parameters of substrates and oxide layers as a function of temperature [(*) pseudo-parameter corresponding to $a^*\sqrt{2}/2$)].

extremly low oxygen pressure (5×10^{-6} Torr) which leads to the reduction of the interfacial silicon oxide by the Ce and Zr atom impinging the Si surface. Metallic Ce and Zr which are very reactive towards oxygen are able to reduce numerous stable oxide such as SiO_x through solid-solid chemical reaction [10,11].

If a decrease of the lattice mismatch between the active perovskite layer and the substrate is needed, the $Ce_{1-x}La_xO_{2-x/2}$ system makes a very attractive oxide family as its in-plane parameter varies between about 0.541 to 0.560 nm (i.e., from 0.383 to 0.396 nm) when the proportion of atomic lanthanum is increasing from 0 to 0.55, i.e., the solubility limit of La_2O_3 in CeO_2 (Fig. 2). We report in the second part of this paper on the effect of this type of buffer layer on the crystallinity, electrical and microwave properties of the subsequently deposited YBCO film. Finally, in the case of $La_{0.7}Sr_{0.3}MnO_3$ hetero-structures, where a buffer layer is unnecessary, as the perovskite is better matched to $SrTiO_3$ ($\Delta a/a = 0.58\%$), a $Ce_{1-x}La_x$-$O_{2-x/2}$ layer matched to the manganese oxide has been tested and compared to $SrTiO_3$ for making only ultra-thin tunneling barrier in a double-hetero-structure dedicated to TMR measurements.

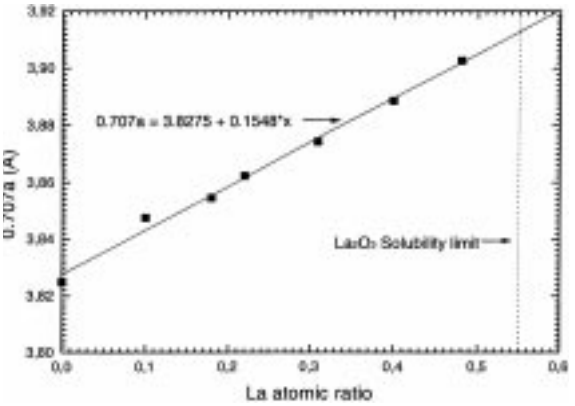

Fig. 2. Lattice parameter ($a^*\sqrt{2}/2$) of $Ce_{1-x}La_xO_{2-x/2}$ as a function of the lanthanum content.

Experimental

Films were prepared *in situ* by PLD in a multitarget LDM 32 Riber machine using a frequency tripled Nd:YAG laser (B.M. Industries 503 DNS) which delivers a laser beam of 355 nm wavelength with a power density of 600 MW/cm^2 after focusing the laser beam on the target. The typical deposition rate is 0.22 nm/s for $SrTiO_3$ and 0.26 nm/s for YBCO at a repetition rate of 2.5 Hz and a substrate-target distance of 33 mm. The ZrCe target is an alloy rod containing 12% of Ce or a ceramic sintered disk, the CeO_2, $Ce_{1-x}La_xO_{2-x/2}$ and YBCO targets are stoechiometric ceramic sintered disks with a density higher than 0.9 of the theoretical one, they are continuously moved to ensure an uniform ablation rate. In contrast to Chambonnet *et al*. [13] who used independant targets of La_2O_3 and CeO_2 for growing $Ce_{1-x}La_xO_{2-x/2}$ buffer layers, it has been decided to work with stoechiometric targets adjusted for the desired La content, taking into account the perfect transfer of the mixed oxide stoechiometry that we observed in a previous study [13,14].

Before the growth, the substrates are cleaned by heating in pure oxygen up to 800°C for 10 min at a pressure of 0.3 Torr. After this cleaning procedure, cleanliness and flatness of the surface are verified by RHEED before starting the growth procedure. The substrate temperature is set between 650 and 780°C and the pressure between 1×10^{-6} and 0.35 Torr depending on the oxide to be grown. During YBCO and LSMO deposition, the substrate holder was continuously rotated at 45 rpm in order to improve the uniformity of the thickness and the composition.

At the end of the deposition, the pressure was increased to 300 Torr. The sample was then cooled to room temperature during a period of 45 min which included an intermediate temperature plateau at 400°C for 15 min.

The surface resistance (Rs) measurements were carried out at 77 K and 10 GHz by the dielectric resonator method using titanium oxide (TiO_2) as a dielectric. The diameter and the thickness of the resonator are 7 and 1 mm respectively, its dielectric contant is 105 with a loss coefficient of 1×10^{-5} at 77 K [15,16]. The Rs values are measured on 400 nm thick YBCO films and are given without any thickness correction.

XRD analysis has been carried out by using $\theta/2\theta$ and 4-circle X-ray diffractometers in Bragg-Brentano-geometry with CuKα sources.

Results and Discussion

Deposition on (1 0 0) Si

The RHEED pattern of the $Zr_{1-x}Ce_xO_2$ layer deposited at 750°C under 5×10^{-5} Torr of pure oxygen on (0 0 1) Si recorded as a function of the deposition time is given in Fig. 3. In contrast to that is observed for the growth of $SrTiO_3$ on MgO [17]), one

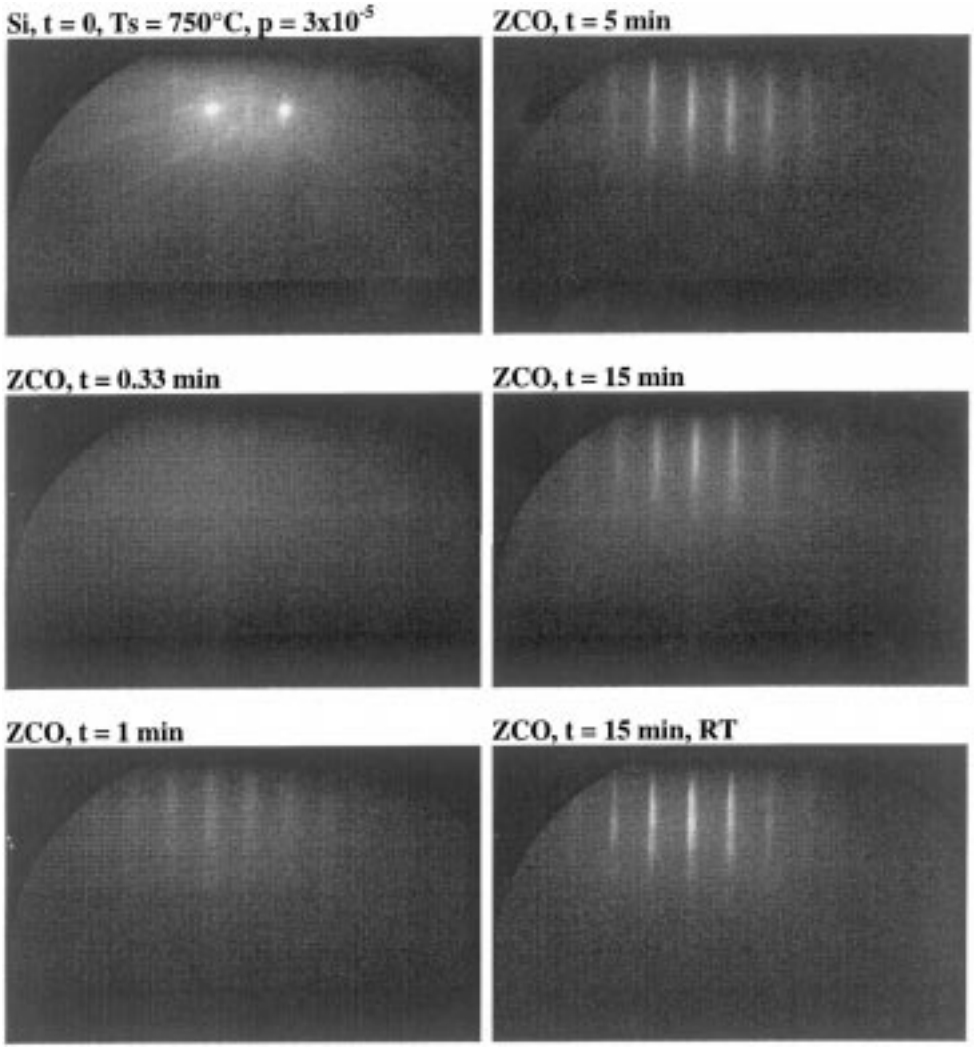

Fig. 3. RHEED pattern recorded along azimuth (1 0 0) of Si during the deposition of $Zr_{1-x}Ce_xO_2$ from a ZrCe metallic target as a function of the time ($Ts = 750°C, P_{O_2} = 3 \times 10^{-5}$ Torr).

must deposit a thick buffer layer (>100 nm) before recovering the diffraction pattern of a flat surface. The XRD $\theta/2\theta$ pattern shows that the layer is epitaxied and oriented with the (0 0 L) axes perpendicular to the substrate surface. The surface of the film deposited from a metallic target (Rrms $= 0.261$ nm) is significantly flatter than that deposited from a sintered ceramic target (Rrms $= 0.343$ nm) as shown in the AFM picture (Fig. 4). The resistive transition of 150 nm thick YBCO layers deposited on $Zr_{1-x}Ce_xO_2$ buffered Si is observed between 88 and 89 K, the transition width being around 2 K. This result is as good as those reported by using an YSZ/CeO_2 double buffer layer [8].

In the case of $La_{0.7}Sr_{0.3}MnO_3$, we show in Fig. 5(a) the magnetization versus field curve at room temperature by AGFM of a film deposited on this buffered Si substrate. The hysteresis loop is quite square with a small coercive field value of 2 mT very close to that obtain by Trajanovic et al. [18], and a small saturation field about 30 mT. At 5 K, the hysteresis loop, measured with a SQUID magnetometer, is composed of a square part with a coercive field of 17 mT and a long tail which does not saturate even in 5 T. This may be due to some inhomogeneities in the sample or to some canting of the magnetization at the surface. This tail is perhaps also present at room temperature

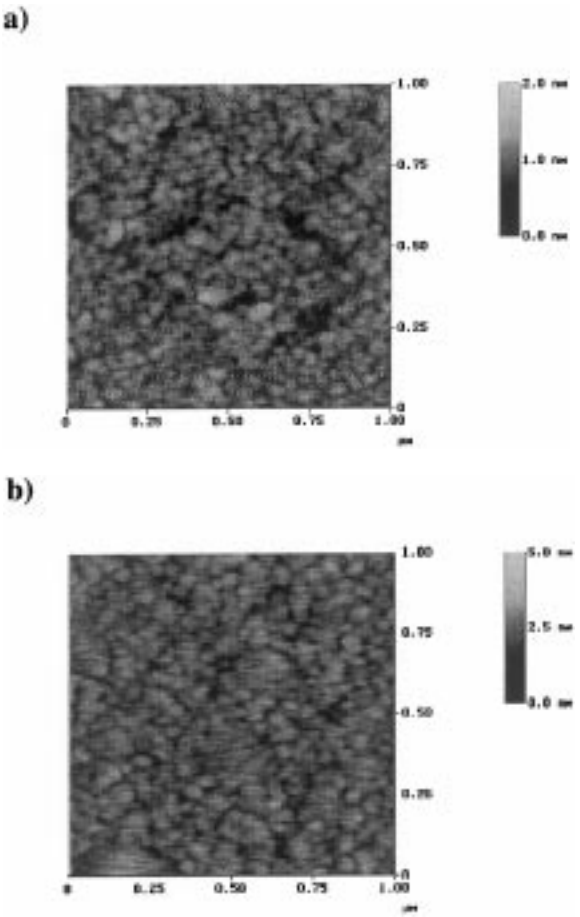

Fig. 4. Atomic force microscopy (horizontal scale $= 1\,\mu$m, vertical scale $= 5$ nm) of a 150 nm thick $Zr_{1-x}Ce_xO_2$ layer deposited on Si (1 0 0) at 750°C under 3×10^{-5} Torr of oxygen: (a) from a metallic alloy target (Rrms $= 0.261$ nm), (b) from an oxide sintered target (Rrms $= 0.343$ nm).

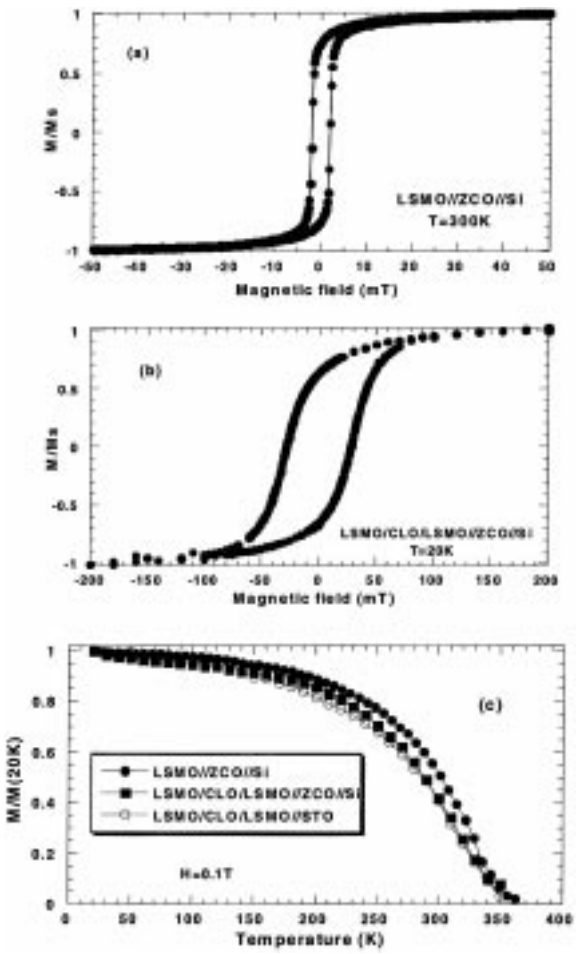

Fig. 5. Magnetization charts versus field and temperature of (a) a $La_{0.7}Sr_{0.3}MnO_3$ film on (1 0 0) Si and (b) $La_{0.7}Sr_{0.3}$-$MnO_3/SrTiO_3/La_{0.7}Sr_{0.3}MnO_3$ double hetero-structure on (1 0 0) Si. In part (c) the magnetization versus temperature dependence of the thin LSMO film, the trilayer LSMO/CLO/LSMO and that of a similar trilayer deposited on an $SrTiO_3$ substrate is shown.

but is not observable by the AGFM measurements performed. A $La_{0.7}Sr_{0.3}MnO_3/Ce_{1-x}La_xO_{2-x/2}/La_{0.7}Sr_{0.3}MnO_3$ (LSMO/CLO/LSMO) trilayer was also deposited on this buffered Si substrate in order to perform, in the future, tunneling magnetoresistance experiments. To optimize the magnetoresistance ratio, large magnetization of the magnetic layers at room temperature is desirable. Figure 5(b) shows the magnetization versus field curve obtained on this trilayer. With relatively large saturation (~ 0.12 T) and coercive (0.03 T) fields and a residual value at zero field of the order of 0.7 that of the saturation value, this hyteresis loop is typical of a polycristalline sample. This polycristallinity has been confirmed by TEM experiments. In Fig. 5(c) we compare the magnetization versus temperature dependence of the thin LSMO film, the trilayer LSMO/CLO/LSMO and that of a similar trilayer deposited on an $SrTiO_3$ substrate. As one can see, the thermal dependence of the three samples is very close, with a critical temperature (T_C) around 350 K. This value is close to the bulk T_C ($\sim$ 370 K), reflecting the good quality of the $La_{0.7}Sr_{0.3}MnO_3$ layers in these structures.

2. $Ce_{1-x}La_xO_{2-x/2}$ ($x = 0.22$) *Buffer Layer for* $YBa_2Cu_3O_7$ *Thin Films*

$Ce_{0.78}La_{0.22}O_{1.89}$ buffer layer matched to the tetragonal phase of YBCO ($a = 0.3866$ nm) have been grown both on (1 0 0) $SrTiO_3$ and $LaAlO_3$ substrates in order to reduce the in-plane residual stress which is observed in this highly mismatched system [4,19]. The $Ce_{1-x}La_xO_{2-x/2}$ growth parameters were first optimized from the RHEED observations. A 2D growth on $SrTiO_3$ is obtained within the temperature range from 680 to 750°C if the oxygen pressure is lower than 10^{-2} Torr, whereas one observed the weak spotty pattern of a 2D–3D growth on $LaAlO_3$ independendly of pressure in contrast to that is observed in the growth of CeO_2 buffer layer (Fig. 6) [13]. As the AFM roughnesses are both low, $Rrms(SrTiO_3) = 0.236$ nm and $Rrms(LaAlO_3) = 0.312$ nm (Table 1), it is assumed that this 3D trend is a consequence both of the lattice mismatch ($\Delta a/a = 2\%$) and the surface texture, due to the drastic twinning of $LaAlO_3$ which is a result of the transition between rhombohedra and cubic structure at 510°C.

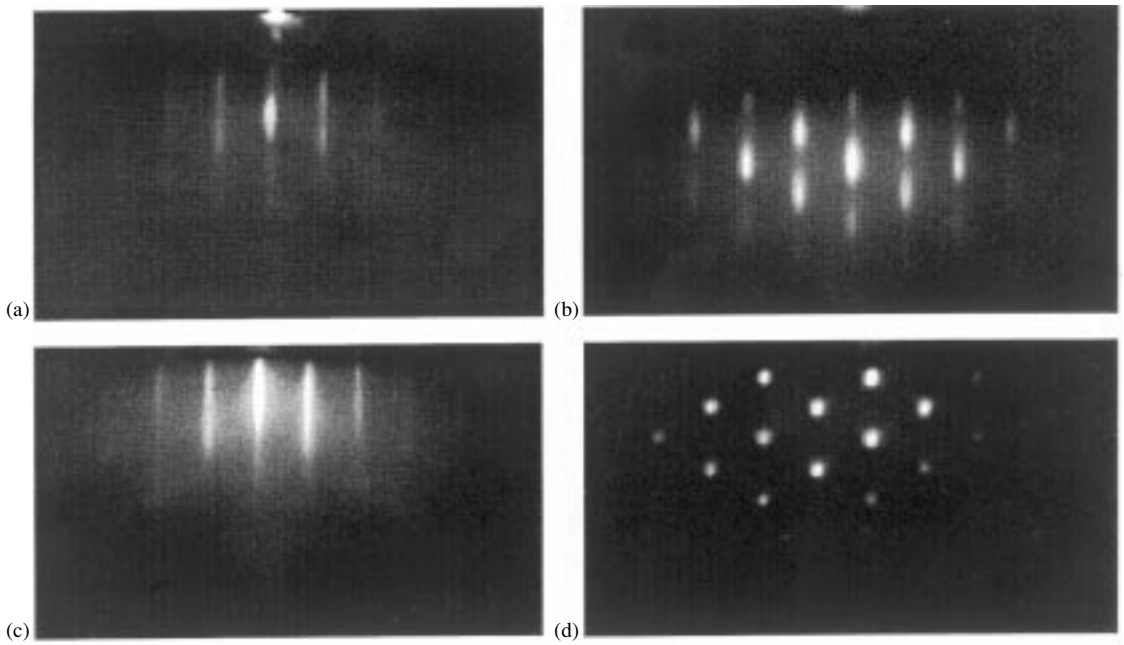

Fig. 6. RHEED pattern recorded at the end of the growth of 250 nm thick $Ce_{1-x}La_xO_{2-x/2}$ films along the (1 0 0) azimuth of the substrate.
(a) $CeO_2/LaAlO_3$ Ts = 700°C, $P_{O_2} = 5 \times 10^{-3}$ Torr
(b) $Ce_{0.78}La_{0.22}O_{1.89}/LaAlO_3$ Ts = 700°C, $P_{O_2} = 5 \times 10^{-3}$ Torr
(c) $Ce_{0.78}La_{0.22}O_{1.89}/SrTiO_3$ Ts = 700°C, $P_{O_2} = 5 \times 10^{-3}$ Torr
(d) $Ce_{0.78}La_{0.22}O_{1.89}/SrTiO_3$ Ts = 700°C, $P_{O_2} = 0.3$ Torr

Table 1. Atomic force microscopy analysis of oxide buffer layers deposited on different substrates

Buffer oxide (thickness nm)	Substrate	Deposition pressure (Torr)	Rrms (nm/1 μm^2)	Rmax (nm/1 μm^2)
$Zr_{0.88}Ce_{0.12}O_2$ Alloy target (1 5 0)	(1 0 0) Si	3×10^{-5}	0.261	4.178
$Zr_{0.88}Ce_{0.12}O_2$ Oxide target (1 5 0)	(1 0 0) Si	3×10^{-5}	0.343	6.072
$Ce_{0.69}La_{0.31}O_{1.845}$ (2 5 0)	$SrTiO_3$	5×10^{-3}	0.236	2.357
$Ce_{0.69}La_{0.31}O_{1.845}$ (2 5 0)	$SrTiO_3$	0.300	0.770	7.45
$Ce_{0.69}La_{0.31}O_{1.845}$ (2 5 0)	MgO	5×10^{-3}	0.640	5.98
$Ce_{0.78}La_{0.22}O_{1.89}$ (2 5 0)	$LaAlO_3$	5×10^{-3}	0.312	3.625

The result of the XRD analysis which was perfomed after the deposition of YBCO on buffered substrates are summarized in Table 2. The films are perfectly oriented with the *c*-axis perpendicular to the substrate surface, no a-perpendicular orientation is detected. In the case of YBCO film deposited on $Ce_{1-x}La_xO_{2-x/2}$ buffered $SrTiO_3$, it should be noted that the FWHM of the rocking curve of the (0 0 5) line is markedly broader than that of the film deposited on buffered $LaAlO_3$, or on unbuffered substrates.

The Φ-scan of the (1 0 2) and (2 2 7) reflection lines confirms a slight increase in the FWHM of these lines and a significant decrease of the preferential rate of [1 1 0] twinning which tends towards the regular rate of 50%. Finally, the Φ-scan of the (1 1 1) reflection of the buffer layer confirms a double 45° in-plane rotation of the epilayers: the buffer axes are rotated of 45° with respect to the substrate axes, but the the YBCO layer rotates a further 45° with respect to the $Ce_{1-x}La_xO_{2-x/2}$ layer so that the YBCO [1 0 0] axis is parallel to the [1 0 0] axis of the substrate (Fig. 7).

The RBS analyses in channeling geometry which are summarized in Table 3 show that the epitaxial relation between the $Ce_{1-x}La_xO_{2-x/2}$ and the substrate is perfect in the case of $SrTiO_3$, the minimun channeling yield at 2.5% being very close to that of the substrate around 1.9% [20] and markedly lower than that of YBCO layers deposited on the same substrate. The χ_{min} at 5.25% which is observed after the growth of the YCBO film on the buffer layer is roughly the same as that measured without buffer, it can then be thought that the buffer does not improve significantly the cristallinity of the YBCO films. On the other hand, the poorer epitaxial relation, which is obtained with $LaAlO_3$ ($\chi_{min} = 8\%$), results in a less perfect relation with YBCO.

The electrical and microwave properties of the YBCO layers are summarized in Table 4. The $Ce_{1-x}La_xO_{2-x/2}$ buffer does not affect transition temperatures and surface resistances but it decreases markedly the the Rs dependence on the magnetic field from 0.009 mΩ/Oe to 0.0038 mΩ/Oe for $LaAlO_3$ substrates, which is especially interesting for microwave applications. On the contrary in the case of MgO

Table 2. Summary of the XRD analysis

Sample	Parameter YBCO (nm)	FWHM (0 0 5) (degree)	FWHM (1 0 2) (degree)	FWHM (2 2 7) (degree)	Twinning rate <1 1 0> (2 2 7)	Parameter $Ce_{0.78}La_{0.22}O_{1.89}$ (nm)	FWHM (1 1 1) (degree)
YBCO/$LaAlO_3$ (100 nm)	$a = 0.3829$ $b = 0.3889$ $c = 1.1699$	0.285	0.67/0.71	0.62/0.63	61%/39%		
YBCO/$LaAlO_3$ (400 nm)	$a = 0.3830$ $b = 0.3896$ $c = 1.1687$	0.288	0.56/0.57	0.49/0.51	56%/44%		
YBCO/$Ce_{0.78}La_{0.22}O_{1.89}$/$LaAlO_3$ (400/250 nm)	$a = 0.3830$ $b = 0.3895$ $c = 1.1698$ $c = 0.5486$	0.292	0.63/0.64	0.58/0.60	51%/49%	$a = b = 0.5486$	0.77
YBCO/$Ce_{0.78}La_{0.22}O_{1.89}$/$SrTiO_3$ (160/250)	$a = 0.3825$ $b = 0.3889$ $c = 1.1687$	0.430	0.75/0.77	0.59/0.57	51%/49%	$a = b = 0.5480$ $c = 0.5484$	0.71

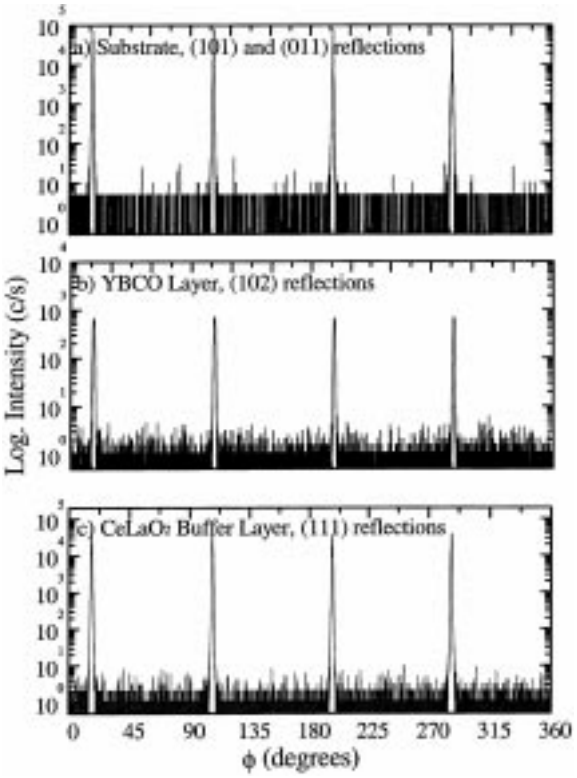

Fig. 7. XRD Φ-scan of a 160 nm thick YBCO layer deposited on a 250 nm thick $Ce_{0.78}La_{0.22}O_{1.89}$ on $SrTiO_3$. (a) substrate (101) and (011) reflections, (b) YBCO, (102) reflections (c) $Ce_{0.78}La_{0.22}O_{1.89}$ buffer layer, (111) reflections.

substrates, whatever the thickness, the $Ce_{1-x}La_x$-$O_{2-x/2}$ buffer layer causes deterioration in the microwave properties of the YBCO film in contrast to that we reported previously on the effect of $SrTiO_3$ buffer layer deposited on MgO [14]. The lowering of the field dependence is may be due to the symmetrization of the [1 1 0] twinning rate which approaches the regular one of 50/50 and possibly decreases the number of high angle grain boundary junctions.

$Ce_{1-x}La_xO_{2-x/2}$ $(x = 0.31)$ *Barrier in* $La_{0.7}Sr_{0.3}MnO_3$ *Double Hetero-Structure*

Several previous papers have reported that extremly high low field magnetoresistance can be obtained in $La_{0.7}Sr_{0.3}MnO_3$ tunnel junctions (TMR) by using $SrTiO_3$ as tunneling barrier [21,22]. Taking into account, first the high epitaxial relation between $SrTiO_3$ and $Ce_{0.69}La_{0.31}O_{1.845}$, then the perfect lattice matching between $La_{0.7}Sr_{0.3}MnO_3$ and $Ce_{0.69}La_{0.31}O_{1.845}$, we have tried to introduce such cerium lanthanum oxide tunneling barrier into $La_{0.7}Sr_{0.3}MnO_3$ hetro-structures. Figure 8(a) and 8(b) show the TEM picture of a cross-section of 2 $La_{0.7}Sr_{0.3}MnO_3$ tunnel junctions with $SrTiO_3$ and $Ce_{0.69}La_{0.31}O_{1.845}$ barrier respectively. In the case of $SrTiO_3$, one observes a perfect continuity of the epitaxial growth in the [0 0 1] direction through the barrier and then in the second $La_{0.7}Sr_{0.3}MnO_3$ layer, the $SrTiO_3$ barrier being compressively strained to the manganite parameter. On the other hand, the high epitaxial relation between $Ce_{0.69}La_{0.31}O_{1.845}$ and $La_{0.7}Sr_{0.3}MnO_3$ is obtained with a 45° in-plane rotation of the former with respect to the latter as reported here above for YBCO; there lay a parameter mismatch of $\sqrt{2}$ in the growth direction. This

Table 3. RBS analysis in channeling configuration

Sructure	YBCO//STO	CLO//STO	YBCO/CLO//STO	YBCO//LAO	CLO//LAO	YBCO/CLO//LAO
Thickness (nm)	150	250	160/250	400	250	400/250
χ_{min} (%)	5	2.5	5.25	4.9	8	8

Table 4. Electrical and microwave properties

Substrate	Buffer layer (thickness nm)	Tc ($R = 0$)	Rs (77 K, 10 GHz)	$\Delta Rs/\Delta B(10^{-3} * m\Omega/Oe)$
$SrTiO_3$	No	91.5		
$SrTiO_3$	$Ce_{0.78}La_{0.22}O_{1.89}$ (2 5 0)	91.6		
$LaAlO_3$	No	91.0	0.26	9.0
$LaAlO_3$	$Ce_{0.78}La_{0.22}O_{1.89}$ (2 5 0)	90.7	0.29	3.8
MgO	No	89.8	0.40	16.7
MgO	$Ce_{0.78}La_{0.22}O_{1.89}$ (2 5 0)	86.1	>1	—

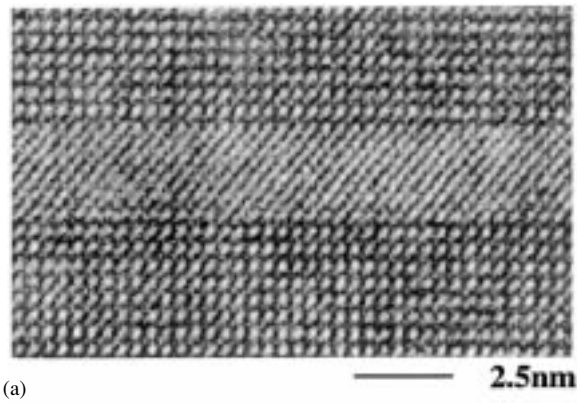

(a)

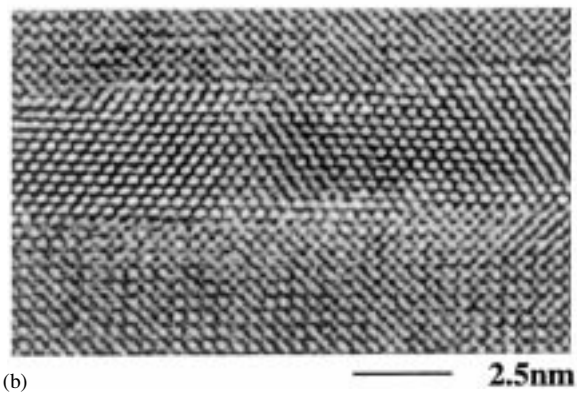

(b)

Fig. 8. TEM cross section of manganite double hetero-structures: (a) $SrTiO_3$ barrier; (b) $Ce_{0.69}La_{0.31}O_{1.845}$ barrier.

mismatch induces strong distortions at each interface step, which propagate into the topmost $La_{0.7}Sr_{0.3}MnO_3$ layer. These deformations are assumed to be at the origin of the drastically lower TMR values which have been observed in preliminary TMR experiments on $La_{0.7}Sr_{0.3}MnO_3/Ce_{0.69}La_{0.31}O_{1.845}/La_{0.7}Sr_{0.3}MnO_3$ hetero-structures in contrast to that obtained with a $SrTiO_3$ barrier (450%) [22].

Conclusion

The Pulsed Laser Deposition of several cerium based oxides has been studied in order to prepare buffer layers dedicated to the epitaxial growth of oxides. The epitaxial growth of $Zr_{1-x}Ce_xO_2$ $(x = 0.12)$ from a metallic target at low pressure on (1 0 0) Si produces a high quality smooth buffer layer $(R_{RMS} = 0.25\,nm/1\,\mu m^2)$ for the oriented growth of $YBa_2Cu_3O_7$ and $La_{0.7}Sr_{0.3}MnO_3$ films, the properties of the perovskite films are as good as those obtained with a double-layer buffer of YSZ and CeO_2. In the case of $Ce_{1-x}La_xO_{2-x/2}(0 \leq x \leq 0.4)$ high quality epitaxial films are obtained on $LaAlO_3$ and $SrTiO_3$, the buffer layers are epitaxially grown with a 45° rotation of the in-plane axes with respect to those of the substrate and the smoothness is high $(R_{RMS} = 0.24\,nm/1\,\mu m^2)$. The properties of YBCO films deposited on these buffered substrates are not significantly improved except the field dependence of the Rs at 77 K and 10 GHz which decreases from $9 \times 10^{-3}\,m\Omega/Oe$ to $3.8 \times 10^{-3}\,m\Omega/Oe$ in the case of $LaAlO_3$ substrates. Finally, the in-plane rotation of the $Ce_{1-x}La_xO_{2-x/2}$ axes increases the interface roughness of ultra-thin barrier ($\cong 2.5$ nm) deposited in $La_{0.7}Sr_{0.3}MnO_3$ hetero-structures by the formation of steps which propagate into the topmost $La_{0.7}Sr_{0.3}MnO_3$ layer in contrast to that is observed for $SrTiO_3$ barriers which produce an ideal crystal continuity parallel to the $<1\,0\,0>$ direction.

Acknowledgments

The authors are grateful to E. Jacquet and M. Mihet for their helpful contribution in the PLD growths and AFM measurements and to J.C. Bombart (C.E.C.M., C.N.R.S.-Vitry) for the ZrCe metallic target preparation. They also thank J. Lesueur (C.S.N.S.M., Université Paris-Sud, Orsay) for the RBS analyzes and B. Marcilhac for valuable help in microwave measurements.

References

1. H.J. Scheel, M. Berkovski, and B. Chabot, *J. Cryst. Growth*, **115**, 19 (1991).
2. H. Koinuma, *MRS Bulletin*, **19**(9), 21 (1994).
3. J.M. Philips, *MRS Bulletin*, **20**, 35 (1995).
4. J.P. Contour, A. Abert, and A. Défossez, *SPIE Proceedings*, **2697**, 339 (1996).
5. H. Nagata, T. Tsukahara, S. Gonda, M. Yoshimoto, and H. Koimuna, *Jpn. J. Appl. Phys.*, **30**, L1136 (1991).
6. H. Koinuma and M. Yoshimoto, *Appl. Surf. Sci.*, **75**, 308 (1994).
7. L. Méchin, J.C. Villégier, G. Rolland, and F. Laugier, *Physica C*, **269**, 182 (1996).
8. S. Zhu, D.H. Lowndes, J.D. Budai, and D.P. Norton, *Appl. Phys. Lett.*, **65**, 2012 (1994).
9. A.G. Akimov, D.B. Bogomolov, A.E. Gorodetskii, L.P. Kazanskii, A.N. Khodan, I.L. Krilov, J.P. Langeron, N.A. Melnikova, D. Michel, J.L. Vignes, and J. Perriere, *Thin Solid Films*, **238**, 15 (1994).

10. T. Hirai, K. Nagashima, H. Koike, S. Matsuno, and Y. Tarui, *Jpn. J. Appl. Phys.*, **35**, 5150 (1996).
11. A Khodan, A.G. Akimov, O. Durand, L.P. Kayanskii, D. Michel, and J.P. Contour, *Eur. Phys. J. A.P.*, **9**, 97 (2000).
12. S. Berger, J.P. Contour, M. Drouet, O. Durand, A. Khodan, D. Michel, and F.X. Régi, *Eur. Phys. J. A.P.*, **1**, 295 (1998).
13. D. Chambonnet, D. Keller, and C. Belouet, *Physica C*, **302**, 198 (1998).
14. Y. Lemaître, L.M. Mercandalli, B. Dessertenne, D. Mansart, B. Marcilhac, and J.C. Mage, *Physica C*, **235–240**, 643 (1994).
15. J.C. Mage and J. Dieumegard, *AGARD Conf. Proceedings*, **481**, 104 (1990).
16. J.P. Contour, C. Couvert, O. Durand, Y. Lemaître, R. Lyonnet, and B. Marcilhac, *Eur. Phys. J. A.P.*, **5**, 3 (1999).
17. Z. Trajanovic, C. Kwon, M.C. Robson, K.C. Kim, M. Rajeswari, R. Ramesh, T. Venkatessan, S.E. Lofland, S.M. Bhagat, and D. Fork, *Appl. Phys. Lett.*, **69**, 1005 (1996).
18. M. Ece, E. Garcia-Gonzales, and H.U. Habermeier, *J. Appl. Phys.*, **77**, 1646 (1995).
19. J. Lesueur, private communication.
20. Y. Lu, X.W. Li, G.Q. Gong, G. Xiao, A. Gupta, P. Lecoeur, J.Z. Sun, Y.Y. Wang, and V.P. David, *Phys. Rev. B*, **54**, R8357 (1996).
21. M. Viret, M. Drouet, J.P. Contour, J. Nassar, C. Fermon, and A. Fert, *Europhys. Lett.*, **39**, 545 (1997).